MIT Libraries | DSpace@MIT

MIT Open Access Articles

Formation and Stability of Impurity "Snakes" in Tokamak Plasmas

The MIT Faculty has made this article openly available. ***Please share*** how this access benefits you. Your story matters.

Citation: Delgado-Aparicio, L. et al. "Formation and Stability of Impurity 'Snakes' in Tokamak Plasmas." Physical Review Letters 110.6 (2013). © 2013 American Physical Society

As Published: http://dx.doi.org/10.1103/PhysRevLett.110.065006

Publisher: American Physical Society

Persistent URL: http://hdl.handle.net/1721.1/78312

Version: Final published version: final published article, as it appeared in a journal, conference proceedings, or other formally published context

Terms of Use: Article is made available in accordance with the publisher's policy and may be subject to US copyright law. Please refer to the publisher's site for terms of use.

Massachusetts Institute of Technology

Formation and Stability of Impurity "Snakes" in Tokamak Plasmas

L. Delgado-Aparicio,[1,2] L. Sugiyama,[3] R. Granetz,[2] D. A. Gates,[1] J. E. Rice,[2] M. L. Reinke,[2] M. Bitter,[1] E. Fredrickson,[1] C. Gao,[2] M. Greenwald,[2] K. Hill,[1] A. Hubbard,[2] J. W. Hughes,[2] E. Marmar,[2] N. Pablant,[1] Y. Podpaly,[2] S. Scott,[1] R. Wilson,[1] S. Wolfe,[2] and S. Wukitch[2]

[1]*PPPL, Princeton, New Jersey 08540, USA*
[2]*MIT-PSFC, Cambridge, Massachusetts 02139, USA*
[3]*MIT-LNS, Cambridge, Massachusetts 02139, USA*
(Received 2 July 2012; published 8 February 2013)

New observations of the formation and dynamics of long-lived impurity-induced helical "snake" modes in tokamak plasmas have recently been carried out on Alcator C-Mod. The snakes form as an asymmetry in the impurity ion density that undergoes a seamless transition from a small helically displaced density to a large crescent-shaped helical structure inside $q < 1$, with a regularly sawtoothing core. The observations show that the conditions for the formation and persistence of a snake cannot be explained by plasma pressure alone. Instead, many features arise naturally from nonlinear interactions in a 3D MHD model that separately evolves the plasma density and temperature.

DOI: 10.1103/PhysRevLett.110.065006 PACS numbers: 52.35.Py, 52.25.Vy, 52.55.Fa

One of the most interesting and commonly observed examples of 3D magnetohydrodynamic (MHD) activity in the core of a magnetically confined fusion plasma is the long-lived helical mode found at the Joint European Torus [1,2] more than 25 years ago. The typical "snakelike" helical patterns observed are characterized by a small region of localized and enhanced plasma density that rotates within the field of view of various diagnostics and is radially concentrated on or inside the $q = 1$ magnetic surface. These long-lived modes are closely associated with sawtooth oscillations of the $q \leq 1$ region and understanding them is potentially important for a burning plasma like the International Thermonuclear Experimental Reactor where the $q = 1$ radius can be as large as half the minor radius. The standard model [3] to describe the snake formation is based on the physics of tearing modes and suggests that the localized cooling of the $q = 1$ surface is responsible for an increase of the local plasma resistivity, which in turn causes a drop in the current density that leads to the formation of a magnetic island with poloidal and toroidal harmonics $m = 1$, $n = 1$. This island is assumed to trap the excess ions from the pellet and form the snake.

Snakes have been a common feature in every major tokamak fusion experiment as well as in spherical tori and reversed field pinches. A second type, produced by an accumulation of impurity ions rather than the deuterium ions from injected fueling pellets, is also observed. Impurity snakes probably appeared first in "type *O*" discharges in Doublet-III [4] and laser-blow-off experiments in the Princeton Large Torus [5]; later examples include the Joint European Torus [2] and the Axially Symmetric Divertor Experiment [6]. Both types of snakes possess surprisingly good MHD stability and particle confinement, since they can survive tens to hundreds of sawtooth cycles. This Letter reports new experimental data on the heavy impurity snakes in the Alcator C-Mod experiment [7], which leads to a new picture of its formation and sustainment as well as its complex relationship with the sawtooth instability. A suite of novel spectroscopic imaging diagnostics has facilitated the identification of the major impurity ion species and the determination of the perturbed radiated power density inside the $q \leq 1$ region with unprecedented temporal and spatial resolution. For the first time, it is possible to infer the impurity ion density, electron temperature, Z_{eff}, and resistivity of the $n = 1$ helical structure. These results can also shed light on the formation and stability of pellet-induced snakes.

Helical snakes like the two depicted in Fig. 1 have been observed in C-Mod Ohmic discharges during the plasma current ramp-up phase or early in the plasma current flattop, where the high edge temperature increases the high-Z impurity erosion from the inner wall (e.g., molybdenum limiter), and the absence of sawtooth crashes allows on-axis impurity peaking. An example of the formation of such—apparently—spontaneous phenomena [2] is depicted in Fig. 1(a) using the time-history of the soft x-ray (SXR) brightness profiles. The second snake shown in Fig. 1(b) had nearly identical radiation profiles until an inadvertent high-Z impurity injection at 0.324 s–10 ms before the snake formation—nearly tripled its radiated power density (P_{rad}) at midradius [compare Figs. 2(a) and 2(b)]. A common feature is, thus, the presence of an initial centrally peaked radiated power density and SXR emissivity due to a strong accumulation of impurities in the plasma core. The identification and localization of the main impurity species was possible using the high resolution x-ray crystal imaging spectrometer with spatial resolution (HiReX-Sr) [8]. Although this diagnostic was designed primarily for extracting temporally and spatially-resolved spectra from argon, it can also monitor intrinsic impurities such as molybdenum;

 © 2013 American Physical Society

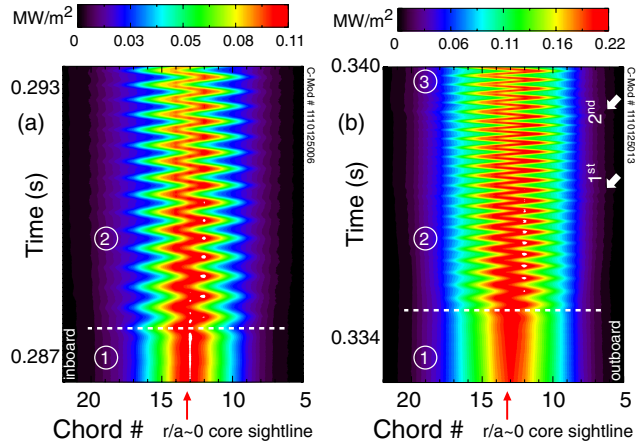

FIG. 1 (color online). Raw SXR brightness profiles of two impurity snakes (a) and (b); horizontal axis is the major radius labeled by vertical viewing chords. The dotted lines indicate the time of their formation while the arrows in (b) indicate the first two sawtooth crashes.

the latter is the main intrinsic high-Z impurity in C-Mod, with an average ion charge $\langle Z_{\mathrm{Mo}}\rangle = 32$ in the plasma core. A detailed comparison between the time-history of the SXR core brightness profiles and the intensity of the Mo^{32+} line has enabled the determination that the net core emission during the impurity peaking and the snake formation is mainly due to molybdenum charge states [8]; consequently, the snakelike pattern in the SXR data shown in Fig. 1 is formed by a small region of localized and enhanced Mo density on or inside the $q = 1$ surface.

The C-Mod snake formation can be described as a three step process corresponding to the numbers in Fig. 1. Stage one, before the snake formation, is characterized by axisymmetric central peaking of the SXR and P_{rad} profiles [see grey profiles for $t \simeq 0.285$ s and $t \simeq 0.334$ s in Figs. 2(a) and 2(b), respectively]. For snake (a) shown in Figs. 1 and 2(a), the core electron density before the impurity accumulation ($t_0 \simeq 0.140$ s, at the end of the current ramp-up phase) is flat and $n_{e0} \simeq 1.2 \times 10^{20}$ m^{-3}, while just before the snake formation ($t_1 \simeq 0.285$ s), it peaks to $n_{e0} \simeq 2.2 \times 10^{20}$ m^{-3}. The net core $P_{\mathrm{rad}} \simeq 2.1$ MW/m^3 then corresponds to a core Mo density

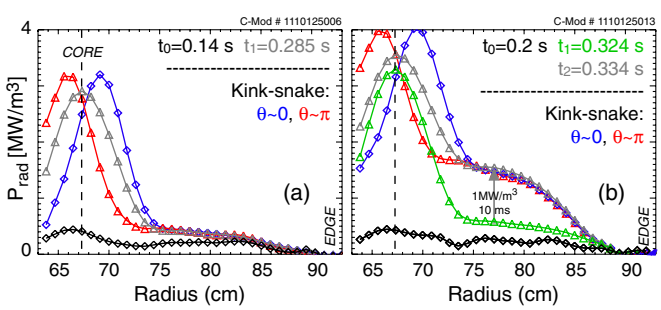

FIG. 2 (color online). Radiated power density profiles before and during the formation (stages one and two) of the two snakes (a) and (b) shown in Fig. 1.

$n_{\mathrm{Mo}} \simeq 1.4 \times 10^{17}$ m^{-3} and a peaked impurity concentration $n_{\mathrm{Mo}}/n_e \simeq 6.3 \times 10^{-4}$; the latter calculation uses a Mo cooling factor $L_{\mathrm{Mo}} \simeq 7 \times 10^{-32}$ W $\cdot$ m^3 [9]. Such an impurity density can increase the core Z_{eff}, as well as the collision frequency ν_{ei} and resistivity η, by more than 50% over the molybdenum-free state. Central values of radiated power density up to $\simeq 3.6$ MW/m^3 have been observed in these discharges and thus, even larger increments of Z_{eff}, ν_{ei}, and η could be expected when compared to molybdenum-free plasmas.

In the second stage, the snake forms as a growing and rotating kinklike $(m, n) = (1, 1)$ helical impurity density concentration with a nearly circular cross section, as shown in the P_{rad} profiles in Fig. 2 and the 2D SXR reconstruction in Fig. 3(a). The latter was obtained at a time step of 4 μs, using a basis of 15 radial Bessel harmonics, a singular value decomposition (SVD) tolerance of 0.1, and a 48 by 84 cm horizontal and vertical emissivity grid with a typical spacing of 1 cm [8,10]; the spatial and poloidal resolution are of the order of 1–2 cm and 10°–20°. This broadly kinked snake precedes any sawtooth onset. The peak SXR and P_{rad} emissivity increase by an additional $\simeq$ (5–10)% (see Fig. 2), since the impurity ions are now confined to a smaller volume. From the net radiated power density and assumed quasineutrality, it is possible to infer the impurity density at the center of the snake $\delta n_{\mathrm{Mo}} \simeq \delta P_{\mathrm{rad}}/n_{e,0}L_{\mathrm{Mo}}$ and its associated electron density perturbation $\delta n_e \simeq Z\delta n_{\mathrm{Mo}}$; a net 2.7 MW/m^3 with a flat core $n_{e0} \simeq 1.7 \times 10^{20}$ m^{-3} will correspond to an increased snake density of $\delta n_{\mathrm{Mo}} \simeq 2.2 \times 10^{17}$ m^{-3} with $\delta n_e \simeq 7 \times 10^{18}$ m^{-3}. The perturbations in density and charge can be as high as $\delta n_e/n_{e,0} \simeq 4\%$ and $\delta Z_{\mathrm{eff}}/Z_{\mathrm{eff},0} \simeq$ (60–70)% (assuming $Z_{\mathrm{eff},0} \simeq 2$). Frequency spectrograms of P_{rad} ($\propto n_{\mathrm{Mo}}$) and electron temperature are depicted in Figs. 4(a) and 4(b). The $n = 1$ nature of the density

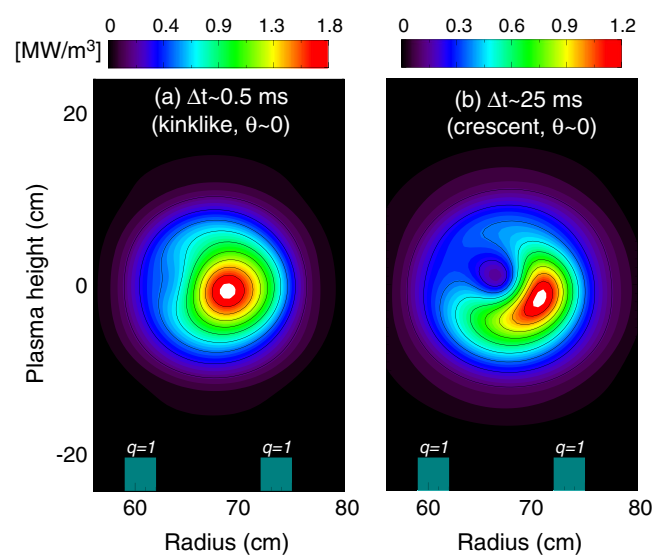

FIG. 3 (color online). Typical SXR emissivity contours during the second and third stages of the snake formation.

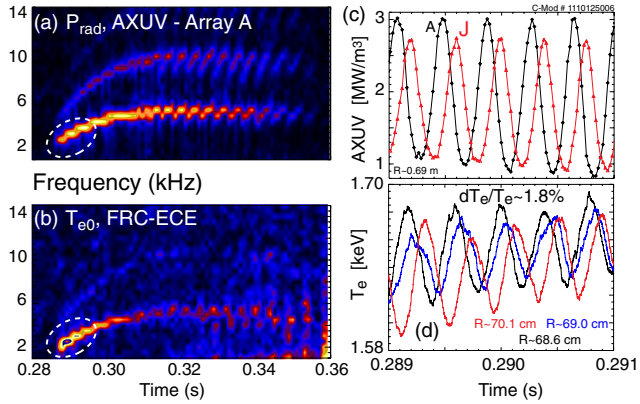

FIG. 4 (color online). Frequency spectrograms of (a) $\tilde{P}_{rad}$ and (b) $\tilde{T}_{e,0}$ core fluctuations in kHz during the formation of the snake (a) in Fig. 1(a). (c) AXUV signals during the stage two snake from two arrays (labeled A and J) displaced 108° in toroidal angle. (d) Values of T_e at three midplane positions.

perturbation has been measured for the first time using using two toroidally displaced AXUV arrays [11] as shown in Fig. 4(c). The phase between the two signals is nearly the same as the geometric angle between the arrays. Typical T_{e0} oscillations measured with an electron cyclotron emission (ECE) radiometer are shown in Fig. 4(d).

The broad, almost circular kink then makes a seamless transition to the third stage, a 1/1 helical structure which resembles the crescent-shaped magnetic island produced by a resistive 1/1 internal kink [see Fig. 3(b)]; this form endures for the life of the snake. Over 50 ms, the typical net radiated power density carried by the snake decreases by $\simeq 1.0\ \mathrm{MW/m^3}$ due to the combined effect of the background transport and sawtooth crashes [8]. The peak snake density decreases by $\simeq 50\%$, while the core electron temperature remains nearly constant at 1.65–1.7 keV (see Fig. 5). The density perturbation narrows steadily and the location of the peak emission moves outwards in minor radius by $\delta r \simeq 2$ cm. The resultant enhanced resistivity

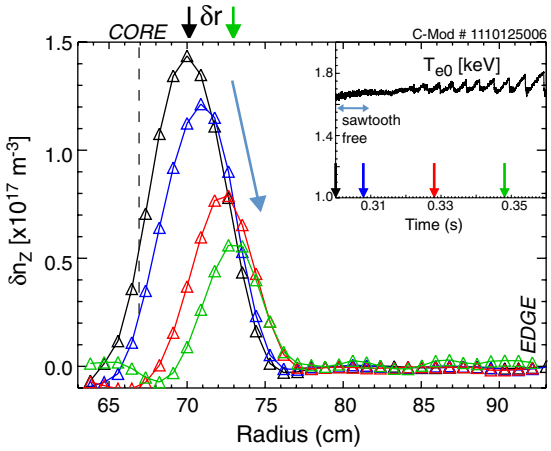

FIG. 5 (color online). Evolution of the impurity density perturbation during the last phase (stage three) of snake (a) from Fig. 1(a).

at the center of the snake, in comparison to that of the background core, decreases from $\delta\eta/\eta_0 \sim \delta Z_{\mathrm{eff}}/Z_{\mathrm{eff},0} =$ 45% to 20%. The high impurity density crescent snake surrounds a smaller circular core of lower impurity density, but higher temperature; this helical crescent density is strongly resilient to sawtooth collapses (see Fig. 6). During the crash, the hotter circular core moves rapidly outwards to the edge of the crescent radius [see white arrow in Fig. 6(b)], where it coincides with an outgoing electron heat pulse. Meanwhile, the peak impurity density of the crescent snake remains nearly unperturbed, showing a decoupling between the dynamics of the temperature (pressure)-driven instability of the core and the snake density. The location of the peak emission shrinks inward by 1–2 cm at the crash. The snake toroidal transit frequency slows by $\simeq 25\%$ at the crash, but later recovers, suggesting a transient change of the toroidal or poloidal flow velocities.

The impurity snake formation departs strongly from the nonlinear island model based on a modified Rutherford equation (MRE), proposed by Wesson [3] and subsequently, applied to impurity snakes [12,13]. The MRE model postulates that a sudden excess of ions at $q = 1$ will induce a

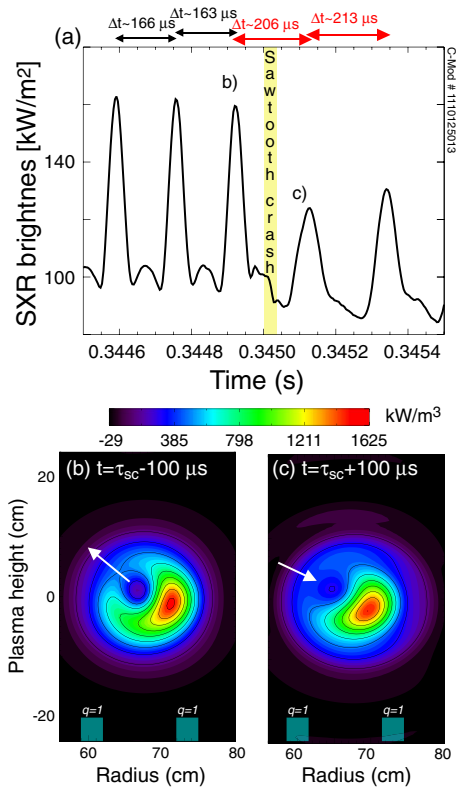

FIG. 6 (color online). Time plot before and after a sawtooth crash in the stage three snake shows (a) SXR brightness of a sightline that intersects the outer edge of the snake. The SXR tomographic reconstructions (b) and (c) were done at the times indicated in (a). Arrows show the direction of motion of the dark lower density (higher temperature) circular core.

"nearly immediate" cooling of the rational surface, which will increase the local plasma resistivity, leading to the formation of a magnetic island. Instead, no evidence for an island is observed during the early C-Mod snake. Moreover, these snakes occur in plasmas with a slow impurity accumulation in the core, with no "instantaneous" cooling. The MRE model, derived for $m \geq 2$ tearing modes, assumes that only conditions at the $q = m/n$ rational surface affect island formation, but the only $m = 1$ instabilities known to produce a $1/1$ magnetic island couple to the entire volume inside $q < 1$. For impurity snakes, the local model also greatly overemphasizes the destabilizing effects of the cooling of the $q = 1$ layer by line and continuum radiation ($P_{\rm rad}$) as well as the change in ion charge ($Z_{\rm eff}$), unlike the case of $m = 2$ NTM magnetic islands [14]. This is shown by the large, destabilizing numbers obtained by Ref. [12]; similar results hold for the C-Mod snake. The saturation of the island, needed to create a sustained snake, then requires that the contribution from the surrounding equilibrium, measured by Δ', be large and stabilizing and remain so during the snake lifetime, a condition that appears to rule out the possibility of sawtooth oscillations.

The likely explanation for the persistence of the snake is that it embodies a quasi–steady-state magnetic structure. The snake's $1/1$ helical configuration and close association with the $q = 1$ surface and ongoing $1/1$ sawtooth crashes suggest that it is related to the $1/1$ internal kink mode [15] with magnetic reconnection. One alternative explanation, based on static ideal MHD equilibria with a 3D helical core [16], reproduces some qualitative features of snakes, but requires strong constraints on the q and pressure profiles. The configurations somewhat resemble the earliest, sawtooth-free stage of the C-Mod snake. However, observed gradual formation from zero amplitude, smooth transition from a broad kink to a crescent shape (very different from the helical core equilibrium), and the details of the periodic sawtooth crashes appear to rule out this type of explanation.

Pressure-based MHD models, with $1/1$ magnetic islands [17,18] or without [16], generally equate the higher snake density with higher pressure. Such models have a fundamental difficulty in explaining the snake's stable coexistence with periodic sawtooth crashes [19]. The internal kink-type instability that causes the crash is driven by the pressure gradient over the $q < 1$ region [15]; nonlinearly, the crash displaces and destroys, or mostly destroys, the high-pressure circular core, thus reducing the drive for the instability. Additional heating of the core (e.g., during the early phase of the Ohmic discharge or the rise phase of the sawtooth) would raise the pressure and destabilize the kink instability. The resulting crash of the core would destroy the snake density concentration along with the core pressure. As the core disappears, the snake density would rapidly flow around the $q = 1$ surface to the poloidally opposite side. Such a phase shift is not observed experimentally [cf. Fig. 1(b)]. On the other hand, higher density and pressure in the crescent island would tend to stabilize the sawtooth [17]. In the later C-Mod snake, such as Fig. 6, T_e observations show that the high density and high temperature fall on opposite sides of the core/crescent division; i.e., the temperature is depressed in the region where the snake density is enhanced. The higher pressure of the higher T_e circular core drives a partial sawtooth crash, but does not greatly affect the snake density contained in the crescent side.

Nonlinear MHD simulations of the early snake in C-Mod-like plasmas [19], using separate temperature and density evolution, suggest that a $1/1$ helical density perturbation localized near $q = 1$ is compatible with the observed early snake formation and also with ongoing sawtooth crashes. For a C-Mod shaped plasma with a small $q < 1$ region and small background toroidal rotation similar to the snake plasmas, the results from the M3D initial value code show that a positive helical density of a few percent, in an annulus peaked around or just outside the $q = 1$ radius, drives a new type of internal kinklike mode inside $q < 1$ (see Fig. 7), in such a fashion as to minimize the perturbed $1/1$ pressure gradient and free energy. Over $q < 1$, the central perturbed pressure and poloidal magnetic flux are closely aligned and resemble a classical $1/1$ internal kink mode [19]. Unlike the classical kink, the density perturbation over $q < 1$ is small so $\tilde{p} \simeq n\tilde{T}$. The total density perturbation has a broad helically kinked shape extending beyond $q = 1$ that resembles the early, stage two C-Mod snake in Fig. 3(a). Over $q \simeq 1$, the temperature tends to be reduced where the perturbed density is large. The density forms a long-lived quasisteady

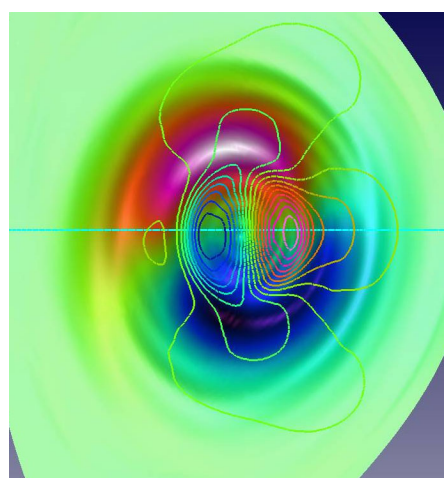

FIG. 7 (color online). Nonlinear MHD simulation shows a slowly growing $1/1$ kink-type mode over $q \lesssim 1$ coupled to a helical density component peaked at or just outside the $q = 1$ radius. Nonaxisymmetric part of δn shown by red [positive (+) → light color]/blue [negative (–) → dark color] shading. Contour lines show a poloidal magnetic flux $\tilde{\psi}$ typical of a $1/1$ internal kink instability; $q = 1$ falls at the outer edge of the closely nested "D" contours. Contours extending outside $q = 1$ represent the $m = 2$ and 3 poloidal harmonics.

structure that is closely tied to the slowly growing 1/1 mode inside $q < 1$. The pressure driven 1/1 kink inside $q < 1$ moves towards positive $\tilde{p}$ or $\tilde{\psi}$, horizontally to the right in Fig. 7. The sawtooth crash it produces will redistribute p, T, and n over $q < 1$ and thus, would have relatively little effect on the peak snake density located at $q \gtrsim 1$. Since in the C-Mod Ohmic plasma the $q = 1$ radius initially grows steadily and axisymmetrically due to the resistive current equilibration, this type of configuration could also be consistent with the gradual transition of the 1/1 density from $q \simeq 1$ into a crescent-shaped concentration trapped in a 1/1 island, e.g., from Figs. 3(a) and 3(b). For a larger and more unstable $q < 1$ region, a similar helical density perturbation can trigger a sawtooth crash [19], seen to initiate some other impurity snakes [2].

In conclusion, a new suite of imaging diagnostics on Alcator C-Mod enables estimates of the $n = 1$ helical structure of P_{rad}, n_{Mo}, n_e, T_e, Z_{eff}, and η inside the $q \leq 1$ region with adequate temporal and spatial resolution. High-resolution observations of heavy-impurity 1/1 snakes show details of their evolution and the accompanying sawtooth oscillations that suggest important differences between the density and temperature dynamics, ruling out purely pressure-driven processes. The observed differences are consistent with nonlinear 3D MHD simulations that evolve plasma density and temperature separately.

This work was performed under US DoE Contract No. DE-FC02-99ER54512 and others at MIT and DE-AC02-09CH11466 at PPPL. Computational support was provided by the National Energy Research Scientific Computing Center under DE-AC02-05CH11231.

[1] A. Weller, A. D. Cheetham, A. W. Edwards, R. D. Gill, A. Gondhalekar, R. S. Granetz, J. Snipes, and J. A. Wesson, Phys. Rev. Lett. **59**, 2303 (1987).
[2] R. D. Gill, A. W. Edwards, D. Pasini, and A. Weller, Nucl. Fusion **32**, 723 (1992).
[3] J. Wesson, Plasma Phys. Controlled Fusion **37**, A337 (1995).
[4] G. L. Jahns, S. Ejima, R. J. Groebner, N. H. Brooks, R. K. Fisher, C. L. Hsieh, T. S. Taylor, J. C. Wesley, N. Fujisawa, and T. Sugawara, Nucl. Fusion **22**, 1049 (1982).
[5] S. Cohen (private communication).
[6] D. Naujoks *et al.*, Nucl. Fusion **36**, 671 (1996).
[7] Alcator C-Mod Team, special issue on "The Alcator C-Mod Program," Fusion Sci. Technol. **51**, No. 3, 261 (2007) [http://www.new.ans.org/pubs/journals/fst/a_1421].
[8] L. Delgado-Aparicio *et al.*, Rev. Sci. Instrum. **83**, 10E517 (2012).
[9] K. B. Fournier, D. Pacella, M. J. May, M. Finkenthal, and W. H. Goldstein, Nucl. Fusion **37**, 825 (1997).
[10] L. Wang, and R. S. Granetz, Rev. Sci. Instrum. **62**, 842 (1991); **62**, 1115 (1991).
[11] M. L. Reinke and I. H. Hutchinson, Rev. Sci. Instrum. **79**, 10F306 (2008).
[12] A.-L. Pecquet, P. Cristofani, M. Mattioli, X. Garbet, L. Laurent, A. Geraud, C. Gil, E. Joffrin, and R. Sabot, Nucl. Fusion **37**, 451 (1997).
[13] Y. Liu *et al.*, in *Proceedings of the 20th IAEA Fusion Energy Conference, Vilamoura, Portugal, 2004*, http://www-naweb.iaea.org/napc/physics/fec/fec2004/papers/ex_p5-12.pdf.
[14] L. Delgado-Aparicio *et al.*, Nucl. Fusion **51**, 083047 (2011).
[15] M. N. Bussac, R. Pellat, D. Edery, and J. L. Soule, Phys. Rev. Lett. **35**, 1638 (1975).
[16] W. A. Cooper, J. P. Graves, and O. Sauter, Nucl. Fusion **51**, 072002 (2011); Plasma Phys. Controlled Fusion **53**, 024002 (2011).
[17] W. Park, D. A. Monticello, and T. K. Chu, Phys. Fluids **30**, 285 (1987).
[18] A. Thyagaraja and F. A. Haas, Phys. Fluids B **3**, 580 (1991).
[19] L. Sugiyama and L. Delgado-Aparicio, in *Proceedings of the 54th Annual Meeting of the APS Division of Plasma Physics, Providence, Rhode Island, 2012*, http://meeting.aps.org/Meeting/DPP12/Event/175996 [Bull. Am. Phys. Soc. (to be published)].